Experimental and numerical determination of the optimal stack position maximizing cooling efficiency in a thermoacoustic refrigerator

A. Carrasco-Gonzaga[a,b,*], G. Dominguez-Librado[a,b,⋆], and L. Del Llano-Vizcaya[a,c,†]

[a]*SECIHTI-Centro de Ingeniería y Desarrollo Industrial,*
Av. Playa Pie de la Cuesta No. 702, Santiago de Querétaro, 76125, Querétaro, México.
[b]*Current address: Laboratorio Nacional de Investigación en Tecnologías del Frío;*
[c]*Gerencia de Simulación Mecánica.*
[*]*e-mail: a.carrasco@posgrado.cidesi.edu.mx; ORCID: 0000-0001-5287-5579,*
[⋆]*0000-0001-9090-5337,*
[†]*0000-0001-6203-5282*

E. E. Rodríguez-Vázquez
Innovación Científica y Tecnología Especializada en Soluciones Industriales,
Prudencia Griffel 714, la Joya. Querétaro, México,
ORCID: 0000-0001-8794-4482.

Received 1 September 2025; accepted 12 November 2025

This paper focuses on studying and determining the appropriate distance for the location of the thermoacoustic stack, one of the basic components of thermoacoustic cooling systems. The position of the stack within the resonator tube is of utmost importance as it allows for the proper production of the thermoacoustic effect and maximizes energy exchange in the thermal boundary layer. The procedure used to determine the optimal position of the stack first describes the operating principle and the equations that govern the thermodynamic cycle. Subsequently, numerical modeling is developed by normalizing the variables involved, performing the best adjustment that allows for maximum energy efficiency of the device. The graph of the numerical solution shows the range of possibilities for the position of the stack and explains how it influences the energy efficiency of the system. The experimental validation process is carried out in a thermoacoustic prototype where two series of tests are performed: the first in a certain region by trial and error, and the second using the value found in the numerical modeling. The variable evaluated is the temperature difference using a thermal camera and temperature sensors. Finally, the results show that the best temperature gradient achieved in the cold zone corresponds to the maximum coefficient of performance evaluated in the prototype.

Keywords: Thermoacoustic refrigeration; optimization; normalization; standing wave.

DOI: https://doi.org/10.31349/RevMexFis.72.030601

1. Introduction

The fundamentals of thermoacoustic refrigeration were established just over two centuries ago, based on the study of sound wave behavior. The first documented findings date back to 1777, when Byron Higgins [1] described a unique phenomenon: when a hydrogen flame was introduced into a glass tube and positioned at a specific point, acoustic oscillations were generated. As a result of these natural convection effects, the open end of the tube emitted an audible sound.

In 1887, Lord Rayleigh offered the first qualitative explanation of this phenomenon. He postulated that vibration is reinforced "if heat is applied to the air at the moment of greatest condensation, or removed at the moment of greatest rarefaction." In practice, this principle means that when heat is supplied to a fluid at its point of maximum compression (maximum acoustic pressure), its temperature increases. Conversely, if heat is removed during the phase of minimum compression (minimum acoustic pressure), the thermal energy of the medium is reduced. This exchange of energy at the precise moment amplifies the original pressure disturbance, thus intensifying the oscillation [2].

In the mid-20th century, scientists began researching the reverse thermoacoustic effect, a phenomenon that uses sound waves to transport heat between two areas via a working fluid, thereby generating a cooling effect. This principle is known as thermoacoustic refrigeration (TAR).Between 1969 and 1980, Rott [3] made fundamental theoretical contributions that laid the foundations for modern thermoacoustics.

The 1997 Kigaly Amendment to the Montreal Protocol established a licensing system to control trade in ozone-depleting substances such as methyl bromide. It also provided for the phasing out of the production and consumption of conventional refrigeration systems using chlorofluorocarbons (CFCs) or hydrochlorofluorocarbons (HCFCs), including existing equipment, which was scheduled to be completely phased out in the following years [4]. These gases, widely used in refrigeration and air conditioning systems, were later identified as harmful to the environment due to their role in ozone depletion. The regulations, applicable to both developed and developing countries [5], spurred the search for and development of alternative, more environmentally friendly refrigeration technologies.

For this reason, TAR has garnered increasing interest from both scientific and industrial sectors. Its appeal lies in the use of an inert gas as the primary working fluid and a solid conductive material as the secondary heat transfer medium, a combination that eliminates adverse environmental effects. This environmentally neutral approach establishes TAR as a sustainable and efficient alternative to conventional refrigeration systems [6].

A typical TAR system operates using sound waves and an inert gas-such as helium, argon, air, or a mixture thereof. Its core components include a cylindrical resonator, an acoustic driver (loudspeaker), a porous element (stack), and two heat exchangers. When the loudspeaker generates sound waves, it creates a resonance phenomenon. As the gas oscillates, its compression and expansion due to acoustic pressure produce a temperature gradient along the stack. This gradient results from the displacement of thermal energy from the cold end to the hot end [7]. Notable research in this field were [8-12].

Most research and development in TAR has been concentrated in the United States, China, and several European countries. This focus stems from a heightened concern in these regions regarding ozone layer depletion and the environmental impact of CO_2 emissions. Consequently, advancing this technology is considered vital for generating a positive environmental impact and mitigating existing damage. The thermoacoustic phenomenon has already been implemented in specific applications, including cryogenics [13], natural gas liquefaction [14], electricity generation [15], domestic refrigeration [16], and the thermal management of electronic devices [17]. The design and optimization of TAR devices are particularly important for developing countries like Mexico, which are expected to face energy and environmental challenges similar to those of industrialized nations in the near future.

TAR is a relatively nascent technology. Despite recent progress, both research and practical applications remain limited, with only a small community of researchers actively working in the field. This leaves substantial room for exploration, particularly concerning the fundamental theoretical principles of thermoacoustic phenomena. Continued scientific advancement is expected to deepen the understanding of component behavior and improve the performance of thermoacoustic prototypes [18]. Consequently, many researchers recognize TAR as a promising alternative with the potential to compete with conventional cooling systems. A critical factor in achieving this competitiveness is the geometric design and fabrication quality of each prototype, which are well-established as crucial determinants of overall performance.

This article outlines a methodology for the experimental validation and optimization of a TAR prototype. The primary objectives are to maximize performance through geometric adjustments and enhance energy efficiency with minimal resource expenditure. By integrating a comprehensive literature review, this work aims to elucidate the technology's potential and promote more sustainable and efficient cooling solutions. This research is currently being developed at LaNITeF (National Laboratory for Research in Cooling Technologies) at CIDESI SECIHTI (CONAHCYT) in Querétaro, México.

2. Conceptual model

The thermoacoustic phenomenon emerges from the dynamic interaction of pressure, velocity, and temperature variations within a confined gas medium. As gas particles oscillate, fluctuations in density and pressure induce corresponding temperature changes in the working fluid. This effect is driven by the coupling between the oscillating gas and the solid boundary of the resonator, where heat is exchanged via conduction. Under these conditions, the acoustic wave becomes spatially confined, generating a temperature gradient along the resonator surface that enables refrigeration. Reversing the direction of heat flow transforms the system into a heat pump [19].

To intensify this temperature gradient, a structured solid element, known as the stack, is positioned within the resonator. The stack facilitates the formation of a high energy zone (hot side, T_h) and a low energy zone (cold side, T_c). Heat exchangers are strategically placed at these locations to inject or extract thermal energy. In certain designs, these exchangers are integrated directly into the stack's geometry to enhance thermal coupling. Based on these principles, a thermoacoustic refrigeration (TAR) prototype consists of the following core components [20], as illustrated in Fig. 1.

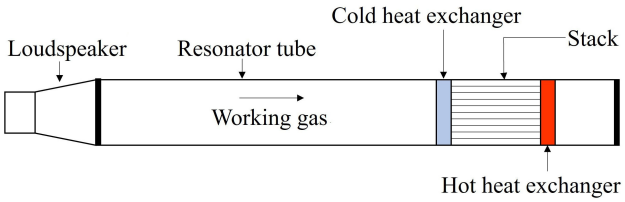

FIGURE 1. Simplified representation of the thermoacoustic refrigeration system, illustrating the acoustic driver, resonator tube, working gas, stack section, and the corresponding cold and hot heat exchangers.

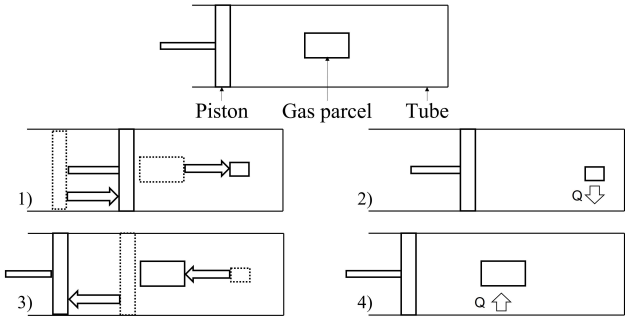

FIGURE 2. Schematic illustration of a gas parcel undergoing the thermoacoustic cycle inside a resonator, showing the successive compression, heat exchange and expansion stages that lead to acoustic-driven thermal transport.

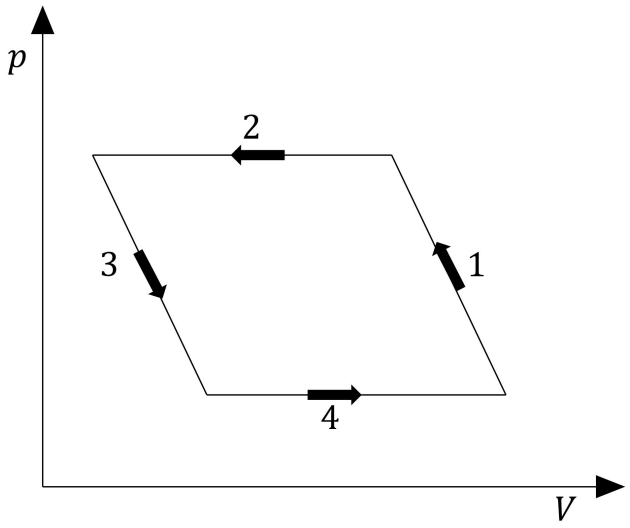

FIGURE 3. Pressure-volume representation of the Brayton-like cycle associated with the thermoacoustic effect, indicating the sequence of compression and expansion processes experienced by the oscillating gas parcel.

2.1. Thermodynamic effect

To aid in understanding the thermoacoustic phenomenon, it is often illustrated using a cylinder-piston analogy. Consider a resonator tube sealed at both ends, one end closed, and the other fitted with a piston that serves as the acoustic driver. Within this system, a small volume of gas, referred to as a "gas parcel", is defined to trace the thermodynamic cycle necessary for the effect to occur [21]. In simplified terms, the piston executes a reciprocating motion, periodically compressing and expanding the gas parcel inside the tube. This dynamic interaction, depicted in Fig. 2, models the fundamental mechanism by which acoustic energy induces thermal gradients.

The thermoacoustic cycle consists of four distinct stages: stages 1 and 3 are adiabatic, while stages 2 and 4 are isobaric. This sequence closely resembles the Brayton thermodynamic cycle, as illustrated in Fig. 3.

Step 1: The cooling mechanism begins when the temperature difference between the inner boundary of the tube and the contained gas element is negligible or absent. At this stage, the piston shifts toward the right, compressing the gas portion and thereby increasing its thermal state.

Step 2: As a consequence of this compression, the gas element acquires a temperature higher than that of the nearby tube surface, leading to the transfer of energy toward the wall.

Step 3: The piston then returns toward the left side of the tube, forcing the gas element to expand while moving in the opposite direction. With reduced internal energy, the gas undergoes a cooling process.

Step 4: As the gas element cools, its temperature becomes slightly lower than that of the tube boundary, which results in a reverse flow of heat from the wall into the gas.

Upon completing the four stages, the gas parcel returns to its initial state, and the cycle repeats. After multiple iterations, a temperature gradient is established along the resonator tube, cooling the piston end and heating the closed end. To harness and control this gradient, a solid geometric structure known as the stack is introduced. Within the stack, the opposing ends undergo cooling and heating, respectively, enabling more efficient thermal management.

2.2. Stack

While the theoretical foundations of thermoacoustics were previously established, they were later expanded and experimentally validated by [22]. The design and analysis of thermoacoustic systems must begin with the stack, as its geometry and placement govern the internal thermodynamic behavior [23]. Various stack configurations have been proposed [24]; in this context, a parallel-plate stack is examined, as shown in Fig. 4. Each plate has a thickness of $2l$, and the spacing between adjacent plates is $2y_0$.

$$B = \frac{y_0}{y_0 + l}. \tag{1}$$

The geometric parameters of the stack are critical, as they define a dimensionless quantity known as the blockage ratio (B). This ratio reflects the proportion of the cross-sectional area occupied by the gas and determines whether the stack achieves equilibrium between thermal and viscous boundary layers as shown in Eq. (1).

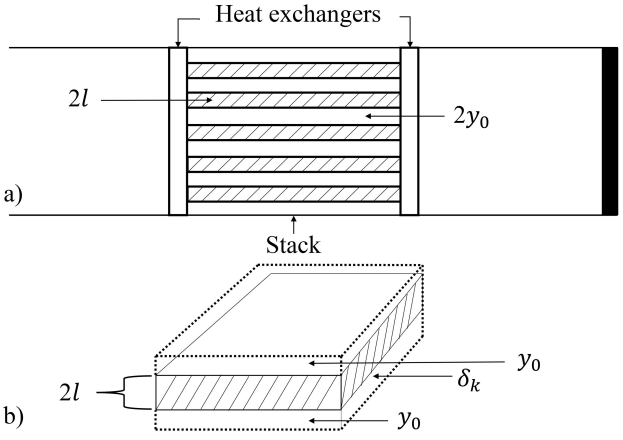

FIGURE 4. a) Cross-sectional representation of the thermoacoustic stack positioned within the resonator, showing its connection with the hot and cold heat exchangers. b) Enlarged schematic of a representative stack element, indicating the plate spacing $2y_0$, plate half-length l, and thermal penetration depth δ_k.

2.3. Governing equations

The transport phenomena that govern the behavior of TAR are described by the Navier-Stokes equation (2), the continuity equation (3), and the energy Eq. (4) [25].

$$\rho\left[\frac{\partial \mathbf{v}}{\partial t}+(\mathbf{v}\cdot\boldsymbol{\nabla})\mathbf{v}\right]=-\boldsymbol{\nabla}p+\mu\boldsymbol{\nabla}^2\mathbf{v}+\left(\xi+\frac{\mu}{3}\right)\boldsymbol{\nabla}(\boldsymbol{\nabla}\cdot\mathbf{v}), \tag{2}$$

$$\frac{\partial \rho}{\partial t}+\boldsymbol{\nabla}\cdot(\rho\mathbf{v})=0, \tag{3}$$

$$\frac{\partial}{\partial t}\left(\frac{1}{2}\rho v^2+\rho\epsilon\right)=-\boldsymbol{\nabla}\cdot\left[\rho\mathbf{v}\left(\frac{1}{2}v^2+h\right)-K\boldsymbol{\nabla}T-\mathbf{v}\cdot\boldsymbol{\Sigma}\right]. \tag{4}$$

where ρ denotes the density, $\mathbf{v}$ is the velocity (u, v, e), μ the dynamic viscosity, ξ the shear viscosity, ϵ the maximum attractive energy, h the specific enthalpy, K the thermal conductivity, and Σ the viscous stress tensor, all defined within the three-dimensional Euclidean space $\mathbb{R}^3$.

However, based on these equations, thermoacoustic theory as it is known today was developed by Rott through various works [26-29], and later reviewed and expanded by Swift [22]. In 2001, Tijani [33] first formulated the equations that describe TAR as a linear system, taking the resonator of the device as the starting point and assuming a one-dimensional model. For this purpose, the following restrictions and boundary conditions were defined:

- Secondary phenomena not directly associated with energy transport, such as acoustic streaming and turbulence, are disregarded.
- The thermoacoustic stack is assumed to consist of plates that remain fixed and mechanically rigid.
- Temperature fluctuations within the thermoacoustic stack are considered negligible in comparison with the absolute temperature.
- The variation of viscosity with temperature is assumed to be insignificant and therefore omitted.
- The oscillatory variables are represented as harmonically dependent on time and governed by a single angular frequency.

The equations by Swift [22], when treated under the aforementioned restrictions and boundary conditions, yield a system of five differential equations that predict the behavior of a thermoacoustic system in a single spatial dimension, referred to as x, ranging from the beginning to the end of the resonator. These equations are numbered (5) through (9), where the subscripts "s," "g," and "m" refer to properties related to the stack, the gas, and the mean characteristics, respectively.

$$\frac{dp_1}{dx}=\frac{-i\rho_m\omega\langle u_1\rangle}{(1-f_v)}, \tag{5}$$

The term dp_1/dx in Eq. (5) refers to the pressure gradient along the resonator, ω is the angular frequency, u_1 denotes the first-order velocity component of the gas parcel, and f_v refers to the viscosity function in Rott's formulation.

$$\frac{d\langle u_1\rangle}{dx}=\frac{-i\omega}{\rho_m a^2}\left[1+\frac{(\gamma-1)}{1+\varepsilon_s}f_k\right]p_1+\frac{(f_k-f_v)}{(1-\sigma)(1+\varepsilon_s)(1-f_v)}\beta\frac{dT_m\langle u_1\rangle}{dx}, \tag{6}$$

The term $d\langle u_1\rangle/dx$ in Eq. (6) refers to the velocity gradient along the resonator, a is the speed of sound in the gas, γ is the ratio of specific heats (isobaric to isochoric), ε_s is the stack heat capacity ratio, f_k corresponds to the thermal term in Rott's function, σ is the Prandtl number, β is the thermal expansion coefficient, and T_m is the mean temperature.

$$\frac{dT_m}{dx}=\frac{\left\{\frac{\dot{E}_2}{A_g}-\frac{1}{2}\operatorname{Re}\left[p_1\langle u_1\rangle\left(1-\frac{(f_k-f_v)}{(1-\sigma)(1+\varepsilon_s)(1-f_v)}\right)\right]\right\}}{\left\{\frac{\rho_m c_p|\langle u_1\rangle|^2}{2\omega(1-\sigma)(1+\varepsilon_s)|1-f_v|^2}\operatorname{Im}\left[f_v+\frac{(f_k-f_v)\left(1+\frac{\varepsilon_s f_v}{f_k}\right)}{(1-\sigma)(1+\varepsilon_s)}\right]-K-\frac{A_s}{A_g}K_s\right\}}. \tag{7}$$

The term dT_m/dx in Eq. (7) refers to the temperature gradient along the resonator. $\dot{E}_2$ is the total power, A is the cross-sectional area, and c_p is the isobaric specific heat.

$$\dot{E}_2=\frac{A_g}{2}\operatorname{Re}\left[p_1\langle u_1\rangle\left(1-\frac{\beta T_m(f_k-f_v)}{(1-\sigma)(1+\varepsilon_s)(1-f_v)}\right)\right]+\frac{A_g\rho_m c_p|\langle u_1\rangle|^2}{2\omega(1-\sigma)(1+\varepsilon_s)|1-f_v|^2}\frac{dT_m}{dx}\times\operatorname{Im}\left[f_v+\frac{(f_k-f_v)\left(1+\frac{\varepsilon_s f_v}{f_k}\right)}{(1+\sigma)(1+\varepsilon_s)}\right]-(A_gK+A_sK_s)\frac{dT_m}{dx}, \tag{8}$$

$$\frac{d\dot{W}_2}{dx} = \frac{1}{2}A_g\,\omega\left[\frac{\beta}{\omega(1-\sigma)(1+\varepsilon_s)}\frac{dT_m}{dx}\,\mathrm{Re}\left(\frac{f_k-f_v}{1-f_v}\,p_1\langle u_1\rangle\right)\right] - \frac{1}{2}A_g\,\omega\left[\frac{\rho_m\,\mathrm{Im}(-f_v)}{|1-f_v|^2}\,|\langle u_1\rangle|^2 + \frac{(\gamma-1)\,\mathrm{Im}(-f_k)}{\rho_m a^2(1+\varepsilon_s)}|p_1|^2\right]. \quad (9)$$

All the terms in Eq. (8) have been previously defined, while in Eq. (9), the term $d\dot{W}_2/dx$ represents the acoustic power used within the resonator.

2.4. Numerical methodology

The equations presented in Sec. 2.3 are formulated in terms of pressure, velocity, temperature, acoustic power, and total power. Collectively, they constitute a system of five differential equations involving complex variables. To solve this system, it is essential to specify appropriate boundary and initial conditions for each equation. Several methodologies exist for addressing this problem:

- Direct numerical integration, where all five differential equations are solved simultaneously using computational platforms such as MATLAB or Python [30].
- Three-dimensional simulation, employing commercial modeling software like ANSYS or SolidWorks to visualize thermoacoustic behavior [31].
- Specialized thermoacoustic modeling, using tools such as DeltaEC, developed at Los Alamos National Laboratory [32].

Each of the aforementioned approaches presents specific limitations tied to fixed parameter values:

- The first method is sensitive to the spatial discretization parameter dx; smaller values increase computational time, while larger values introduce significant numerical errors.
- The second method, although more accurate in terms of numerical stability, demands longer processing times. To mitigate this, simulations are typically confined to a reduced domain.
- The third method addresses both numerical and visualization constraints but requires extensive calibration. Variations in stack position necessitate multiple simulations, with each configuration representing a distinct prototype.

To overcome these limitations, this research proposes a numerical strategy that leverages the most relevant data [33]. This approach enables the exploration of all possible combinations of stack positions and geometries (denoted as B), while integrating secondary variables into unified, normalized parameters. The implementation is based on Eqs. (10) through (13).

$$\Omega = 1 - \sqrt{\sigma}\delta_{kn} + \frac{1}{2}\sigma\delta_{kn}^2. \quad (10)$$

The term Ω is a variable that is used in Eqs. (11) and (12), and δ_{kn} represents the normalized thermal penetration depth.

$$Q_{Cn} = -\frac{\delta_{kn}D^2\sin(2x_n)}{8\gamma(1+\sigma)\Omega}\left(\frac{\Delta T_{mn}\tan(x_n)}{(\gamma-1)BL_{sn}} \times \frac{1+\sqrt{\sigma}+\sigma}{1+\sqrt{\sigma}} - \left(1+\sqrt{\sigma}-\sqrt{\sigma}\delta_{kn}\right)\right). \quad (11)$$

The term Q_{Cn} represents the normalized heat flux in the stack. D is the drive ratio, which ensures the stabilization of the standing wave, and this value should not exceed 3% to avoid turbulence. ΔT_{mn} is the expected normalized temperature difference, x_n represents the normalized position where the stack should be placed, and finally, L_{sn} is the normalized stack length.

$$W_n = \frac{\delta_{kn}L_{sn}D^2}{4\gamma}(\gamma-1)\,B\,\cos^2(x_n) \times \left[\frac{\Delta T_{mn}\,\tan(x_n)}{BL_{sn}(\gamma-1)(1+\sqrt{\sigma})\,\Omega} - 1\right] - \frac{\delta_{kn}L_{sn}D^2}{4\gamma}\,\frac{\sqrt{\sigma}\,\sin^2(x_n)}{B\,\Omega}, \quad (12)$$

The term W_n represents the normalized acoustic power with which the device operates. Finally, to achieve optimal performance, Eqs. (11) and (12) must be related in such a way that the highest possible efficiency is obtained. For this purpose, the coefficient of performance (COP) is used, linking the heat flux and the acoustic power, as shown in Eq. (13).

$$COP = \frac{Q_{Cn}}{W_n}. \quad (13)$$

2.4.1. *Limitations*

To ensure the reliability of results, the normalized system must operate within specific constraints, which can be grouped into three primary categories [33]:

- Acoustic wavelength constraint: The wavelength of the acoustic wave propagating through the resonator must be significantly greater than the length of the stack. This condition allows pressure and velocity to be treated as spatially uniform within the stack, ensuring that the acoustic field remains unaffected by the stack's geometry.

- Penetration depth constraint: The thermal and viscous penetration depths must be smaller than the spacing between adjacent stack plates. This permits the simplification of Rott's functions, enabling certain complex terms to be approximated as unity and thereby reducing computational complexity.

- Temperature gradient constraint: The temperature difference across the stack faces must remain smaller than the mean temperature. Violating this condition leads to singularities in the normalization process, undermining the validity of the computed results.

3. Results and discussion

3.1. Design

Experimental validation was conducted using a TAR prototype mounted on a dedicated test bench. The system comprises a rectangular aluminum base with supporting structures that hold the resonator tube in place. The acoustic driver is an Eighteen Sound loudspeaker (model 8MB400), rated at 250 W with a diameter of 0.15 m. It is coupled to the resonator tube via an aluminum cone that narrows the diameter to 0.1 m. The resonator itself is constructed from transparent acrylic and measures 0.9 m in length, with a closed end on the right side. Inside the tube, a parallel-plate stack fabricated from polylactic acid (PLA), a biodegradable thermoplastic produced via 3D printing, was installed. Ordinary air served as the inert working gas throughout the system. Figure 5 presents an exploded view of the TAR prototype, highlighting key structural components including the acoustic driver and cone, resonator tube, stack section, support base, and closed end.

3.2. Prototype

To initiate the thermoacoustic effect, a Bose PM8500 amplifier was connected to the loudspeaker. A 130 Hz sinusoidal

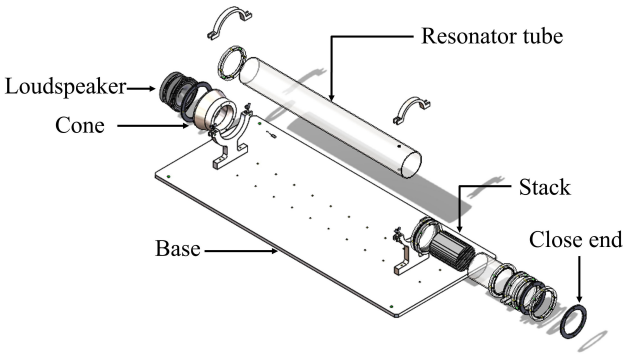

FIGURE 5. Exploded view of the thermoacoustic refrigerator prototype, highlighting the main structural components including the acoustic driver with its cone, resonator tube, stack section, supporting base, and close end.

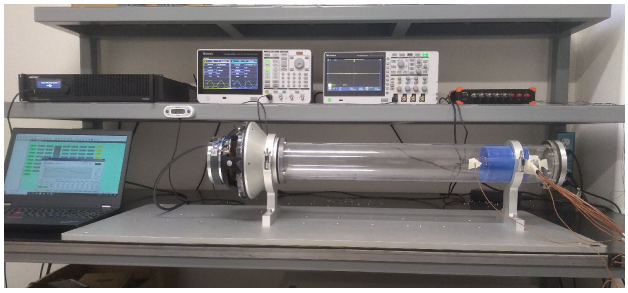

FIGURE 6. Experimental setup of the TAR prototype used for validation tests. The system includes an amplifier connected to a loudspeaker that excites the resonator containing the thermoacoustic stack.

signal, generated by the amplifier's built-in function generator, was used to sustain a standing wave within the resonator. This resulted in the formation of hot (T_h) and cold (T_c) regions at the stack faces. Figure 6 shows the assembled TAR prototype with the stack positioned inside the resonator. Type "T" thermocouples were embedded within the stack to monitor temperature variations. Data acquisition was performed using a National Instruments CRIO-9047 unit paired with a 9214 module, interfaced with a computer. Measurements were recorded every 15 seconds, with the most notable temperature changes occurring approximately every 5 minutes.

3.3. Experimental test

The experimentation involves a comparison between two types of tests, ensuring that the same conditions are maintained throughout. The input variable, x_c, is defined as the position of the center of the stack measured from close end, while the output variable is the cooling temperature reached in the cold zone of the stack.

The first set of tests consists of five trials, in which the distance x_c is determined empirically. A specific interval is selected based on prior observations indicating where the highest temperature gradient is generated, according to the recorded and analyzed temperature data. The goal is to identify the optimal position for the stack's operation.

In this first series of tests, the resulting data collected from the thermocouples on T_h and T_c sides were averaged. The stack was empirically positioned at $x_c = 12$ cm, leaving 7 cm distance between the hot face of the stack and the close

TABLE I. Experimental results showing the average thermal behavior of the stack positioned at $x_c = 12$ cm.

Time (min)	T_h(°C)	T_c(°C)
0	19.85	19.25
5	27.89	19.11
10	30.61	18.68
15	31.62	18.32
20	32.76	17.89
25	32.85	17.85

TABLE II. Main operating parameters and physical properties used in the operation of the TAR prototype.

Parameters	Values	Units
Resonance frequency	130	Hz
Mean pressure	1.101325	Bar
Mean temperature	292.65	K
Speed of sound	344	m/s
Pressure of wave	0.0287	Bar
Dynamic viscosity	0.0000184	kg/ms
Isobaric specific heat	1007	J/kgK
Thermal conductivity	0.024	W/mK
Mean density	1.204	$\mathrm{kg/m^3}$
Plate spacing	0.00055	m
Plate thickness	0.00025	m
Stack length	0.1	m
Normalized parameters		
L_{sn}	0.2374	-
x_n	To find	-
σ	0.772	-
δ_{kn}	0.4003	-
γ	1.2937	-
ΔT_{mn}	0.0444	-
B	0.6875	-
D	0.0261	-

end. The averaged data were recorded and are presented in Table I.

The second set of tests consists of five experiments in which a numerical solution is used to determine the optimal position of the stack through the normalized variable x_n. This parameter defines the appropriate energetic performance, from which it is possible to calculate the optimal position x_c.

The normalization process and numerical solution were carried out as follows: the input data were defined based on the operating parameters of the device, the properties of the working gas, the geometric dimensions and properties of the stack. The data used for this device are presented in Table II.

Using the values from Table II, Eqs. (10) through (13) were programmed into a computer to generate all possible combinations for determining the optimal stack position within the tube and achieving a defined performance.

This calculation allows for the analysis of the desired COP for the device's operation. Figure 7 shows the performance curve of the stack within the device, illustrating its normalized position along the resonator tube (x-axis) versus energy performance (y-axis). In this study, a COP of 3.5976 was selected for the prototype, as it yields the highest performance while minimizing energy losses.

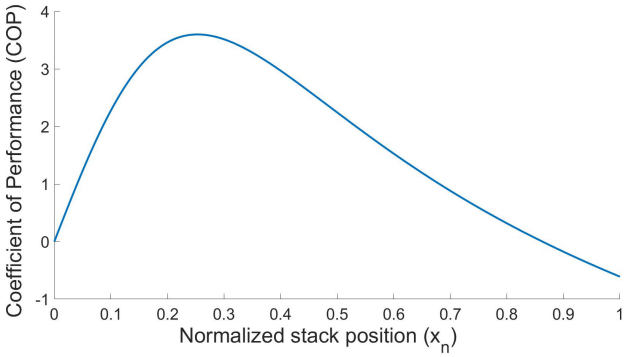

FIGURE 7. Normalized performance curve of a parallel-plate stack along the resonator. The plot shows the coefficient of performance (COP) as a function of the normalized stack position. The optimal configuration corresponds to a normalized position $x_n = 0.253$ and a normalized stack length $L_{sn} = 0.23745$, yielding a maximum COP of 3.5976, this value corresponds to a physical midpoint distance of 10.65 cm from the close end.

TABLE III. Experimental results showing the average thermal behavior of the stack positioned at $x_c = 10.65$ cm.

Time (min)	T_h(°C)	T_c(°C)
0	19.01	19.5
5	24.8	14.67
10	26.98	13.65
15	28.35	13.43
20	29.31	13.51
25	29.74	13.6

The selection of the maximum COP value corresponds to $x_n = 0.253$. Since this is a normalized value, it must be converted to its scalar form in order to determine the position that results in the lowest energy losses.

The results from the normalization in this second set of tests indicate that the stack should be positioned at $x_c = 10.65$ cm from the close end, placing the hot side 5.65 cm from the close end. Averaged data from the five trials were again recorded and are shown in Table III.

The energy exchanges between the T_h and T_c sides were validated using a Fluke Thermal Imager, model Ti300 Pro, which confirmed and allowed for detailed observation of the temperature variations measured by the thermocouples, as well as those predicted by the numerical solution. These temperature changes are shown in Fig. 8, where subfigures a) and b) represent the first (empirical) test series, and subfigures c) and d) represent the test series conducted with the applied numerical solution.

Both tests were conducted over a duration of 25 minutes, which was sufficient to reach a steady-state condition (no further changes in the hot and cold sides of the stack), ensuring that the collected data were as unbiased as possible. Consequently, upon completion, the data were averaged with a margin of error of 5%, as recorded in Table I and Table III.

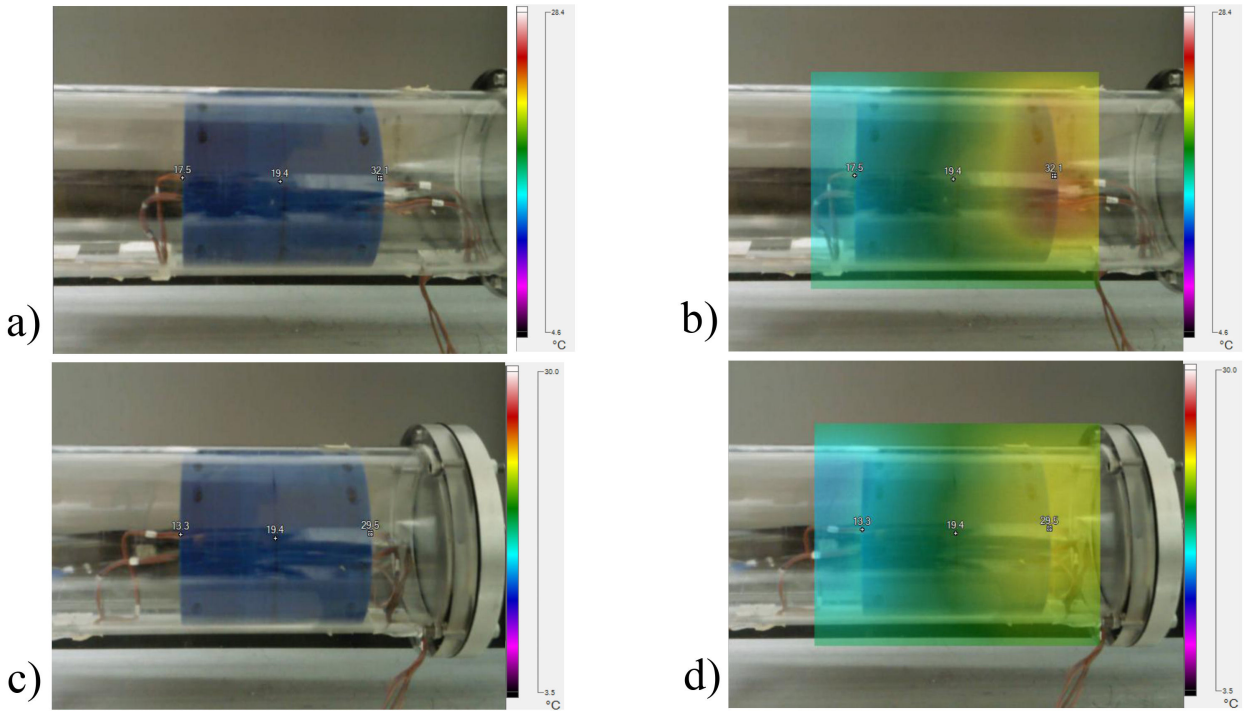

FIGURE 8. Experimental comparison of the thermoacoustic stack performance at two axial positions inside the resonator tube. a) Test at $x_c = 12$ cm b) corresponding thermal mapping at $x_c = 12$ cm c) test at the optimal stack position $x_c = 10.65$ cm d) corresponding thermal mapping at $x_c = 10.65$ cm . The thermal images reveal enhanced cooling performance at the optimal position.

TABLE IV. Experimental record of the empirical tests versus numerical solution results.

Temperature (°C)	Initial value(°C)	Final value(°C)
Experimental record without the solution.		
Ambient temperature	19.85	19.86
T_h	19.85	32.85
T_c	19.25	17.85
T_h vs T_c	0.6	15
Experimental record with the numerical solution.		
Ambient temperature	19.25	19.45
T_h	19.61	29.74
T_c	19.5	13.6
T_h vs T_c	0.11	16.14

The summary of the results is presented in Table IV, where it can be seen that the characterization, construction, stack positioning, and testing were successful in achieving optimal performance of the TAR device using the numerical solution.

4. Conclusions

This research successfully developed and validated a numerical algorithm for optimizing the stack position in a thermoacoustic refrigeration (TAR) device, using a normalized mathematical model. The proposed method yielded enhanced temperature gradients compared to empirical approaches, demonstrating its effectiveness in streamlining the design process.

During empirical optimization, determining the optimal stack location within the resonator required numerous iterations despite the apparent simplicity of the procedure. The best-performing configuration was identified at $x_c = 10.65\,\mathrm{cm}$, where the cold-side temperature decreased by $4.25\,^{\circ}\mathrm{C}$ from $17.85\,^{\circ}\mathrm{C}$ to $13.6\,^{\circ}\mathrm{C}$. Notably, this result was accurately predicted by the numerical model in a single iteration, significantly reducing the time and resources needed during the experimental phase.

The numerical solution enabled direct identification of the optimal stack position, as illustrated in Fig. 7. This prediction guided five experimental tests, which confirmed the repeatability of the results and validated the model's utility for characterizing stack placement in TAR systems.

Implementing an algorithm capable of predicting the optimal stack location ensures a consistent temperature differential across the stack, minimizing energy losses and enhancing the performance of heat exchangers. This approach supports future developments aimed at maximizing energy efficiency and material utilization in thermoacoustic prototypes.

Moreover, the numerical model is adaptable to various TAR configurations, accommodating different working gases, resonator dimensions, and stack geometries (denoted as B, among others) changing values of configuration in Eqs. (10) to (13). Since thermoacoustic behavior is sensitive

to initial operating conditions, each system must be tailored to its environmental context. For instance, the current prototype was designed for the conditions in Querétaro, México; relocating it to a different region would necessitate a redesign to maintain similar performance.

The stack material used a low-cost thermoplastic biopolymer-met the required thermal properties, offering low thermal conductivity and high specific heat capacity.

Overall, the implemented numerical method proved highly efficient, reducing computational demands, simplifying experimental setups, and minimizing the number of field tests required. This optimization capability positions the technology as a promising solution for applications in aerospace, electronics, aeronautics, and biomedical engineering. While initial construction costs may be high, the system's minimal maintenance, due to its lack of moving parts, offers long-term operational advantages.

In conclusion, this research contributes meaningfully to the advancement of emerging refrigeration technologies, particularly in the domains of energy efficiency and system optimization.

Acknowledgments

The authors would like to thank SECIHTI (CONAHCYT) for the support received through the following projects: a) Development of Disruptive Cooling Technology: LaNITeF Infrastructure, FORDECYT-PRONACES 295/20. b) Development of Incremental and Disruptive Technology in Cooling Systems; 322615, 2023-2024. We also express our gratitude to the personnel involved in the administrative management of these projects. We further acknowledge SECIHTI (CONAHCYT) for the scholarship awarded to CVU 1011796, which enabled participation in LaNITeF and the development of this type of technology.

Nomenclature

A	cross-sectional area	m^2
B	stack blockage	$-$
COP	coefficient of performance	$-$
D	drive ratio	$-$
$\dot{E}$	total power	W
K	thermal conductivity	$\mathrm{W/mK}$
L	length	m
T	temperature	K or °C
V	volume	m^3
W	acoustic power	W
a	speed of sound	$\mathrm{m/s}$
c_p	isobaric specific heat	$\mathrm{J/kgK}$
e	z component of velocity	$\mathrm{m/s}$
f	root function	$-$
h	specific enthalpy	$\mathrm{J/kg}$
l	plate half-length	m
p	pressure	Bar
Q	heat flux	W
u	x component of velocity	$\mathrm{m/s}$
v	y component of velocity	$\mathrm{m/s}$
x	position in tube	m
y_0	plate half-spacing	m
β	thermal expansion coefficient	K^{-1}
δ	penetration depth	m^{-1}
ϵ	maximum attractive energy	$-$
γ	isobaric to isochoric ratio	$-$
μ	dynamic viscosity	$\mathrm{kg/(m\,s)}$
ρ	density	$\mathrm{kg/m}^3$
σ	Prandtl number	$-$
ξ	shear viscosity	$\mathrm{kg/(m\,s)}$
ω	angular frequency	$\mathrm{rad/s}$
	subscripts	
C	Carnot	-
c	cold or center	-
g	gas	-
h	hot	-
k	thermal	-
m	mean	-
n	normalized	-
v	viscous	-
s	stack	-
1	first order	-
2	second order	-

1. B. Higgins, On the sound produced by hydrogen gas, *Nicholson's J.* **1** (1802) 130.
2. H. A. Kramers, Vibrations of a gas column, *Physica* **15** (1949) 971-984.
3. N. Rott, Thermoacoustics, *Adv. Appl. Mech*. **20** (1980) 135-175.
4. K. M. Sarma, G. M. Bankobeza y M. A. Mulumba, The Montreal Protocol on Substances that Deplete the Ozone Layer United, Ozone Secretariat, Nairobi, Kenya (1990).
5. G. Domínguez-Librado, E.E.R. Vázquez, L.A.M. Santiyanes, J.H.P. Vázquez and C.A.N. Martín, Transient analysis of a single-stage vapor compression refrigeration system using lumped parameter approaches, *Int. J. Adv. Syst. Meas*. **11** (2018) 352-362.
6. S.L. Garrett, J.A. Adeff and T.J. Hofler, Thermoacoustic refrigerator for space applications, J. Thermophys. Heat Transf. **7** (1993) 595-599, https://doi.org/10.2514/3.466.
7. P. C. Bansod y A. S. Raut, Review on thermoacoustic refrigeration, *Int. J. Innov. Eng. Sci*. **2** (2017) 18-24, https://www.ijies.net/download/review-on-thermoacoustic-refrigeration/.
8. B.L. Minner, J.E. Braun and L. Mongeau, Optimizing the design of a thermoacoustic refrigerator, *Proc. Int. Refrig. Air Cond. Conf*. (1996) Paper 343. http://docs.lib.purdue.edu/iracc/343
9. R. S. Reid y G. W. Swift, Experiments with a flow-through thermoacoustic refrigerator, *J. Acoust. Soc. Am.* **108** (2000) 2835-2842, https://doi.org/10.1121/1.1323721.
10. M. E. H. Tijani, J. C. H. Zeegers y A. T. A. M. de Waele, Construction and performance of a thermoacoustic refrigerator, *Cryogenics* **42** (2002) 59-66, https://doi.org/10.1016/S0011-2275(01)00180-1.
11. A. Campo, M. M. Papari y E. Abu-Nada, Estimation of the minimum Prandtl number for binary gas mixtures formed with light helium and certain heavier gases: Application to thermoacoustic refrigerators, *Appl. Therm. Eng.* **31** (2011) 3142-3146, https://doi.org/10.1016/j.applthermaleng.2011.05.002.
12. T. J. Hofler, Thermoacoustic refrigerator design and performance, Ph.D. Thesis, University of California, San Diego (1986).
13. W. Dai, E. Luo, J. Hu y H. Ling, A heat-driven thermoacoustic cooler capable of reaching liquid nitrogen temperature, *Appl. Phys. Lett.* **86** (2005) 224103, https://doi.org/10.1063/1.1941472
14. J. J. Wollan, G. W. Swift, S. N. Backhaus y D. L. Gardner, Development of a thermoacoustic natural gas liquefier, Los Alamos National Laboratory Report No. LA-UR-01-2652 (2002), https://digital.library.unt.edu/ark:/67531/metadc724978/
15. S. Backhaus, E. Tward y M. Petach, Traveling-wave thermoacoustic electric generator, *Appl. Phys. Lett*. **85** (2004) 1085-1087, https://doi.org/10.1063/1.1781739
16. E. Luo, W. Dai, Y. Zhang y H. Ling, Thermoacoustically driven refrigerator with double thermoacoustic-Stirling cycles, *Appl. Phys. Lett*. **88** (2006) 074102, https://doi.org/10.1063/1.2176855
17. O. G. Symko, E. Abdel-Rahman, Y. S. Kwon, M. Emmi y R. Behunin, Design and development of high-frequency thermoacoustic engines for thermal management in microelectronics, *Microelectron. J.* **35** (2004) 185-191, https://doi.org/10.1016/j.mejo.2003.09.017
18. A. Piccolo, Optimization of thermoacoustic refrigerators using second law analysis, *Appl. Energy* **103** (2013) 358-367, https://doi.org/10.1016/j.apenergy.2012.09.044
19. M.A. Alamir y N.A.C. Sidik, Thermoacoustic refrigerators and heat pumps: New insights for a high performance, *J. Adv. Res. Fluid Mech. Therm. Sci*. **78** (2021) 146-156, https://doi.org/10.37934/arfmts.78.1.146156.
20. G. Domínguez-Librado, C. A. Escalante y L. Del Llano Vizcaya, Modelación numérica y validación experimental del efecto termoacústico en un prototipo de refrigeración, Memorias del XXIX Congreso Internacional Anual de la SOMIM, artículo A4-55 (2023), https://somim.org.mx/memorias/memorias2023/articulos/M58-A4_55.pdf.
21. G.W. Swift, Thermoacoustic engines and refrigerators, *Phys. Today* **48** (1995) 22-28, https://doi.org/10.1063/1.881466
22. G. W. Swift, Thermoacoustic engines, *J. Acoust. Soc. Am.* **84** (1988) 1145-1180, https://doi.org/10.1121/1.396617.
23. M. Wetzel and C. Herman, Design optimization of thermoacoustic refrigerators, *Int. J. Refrig.* **20** (1997) 3-21, https://doi.org/10.1016/S0140-7007(96)00064-3
24. P.S. Bhansali, P.P. Patunkar, S.V. Gorade, S.S. Adhav and S.S. Botre, An overview of stack design for a thermoacoustic refrigerator, *Int. J. Res. Eng. Technol*. **4** (2015) 68-72.
25. G.W. Swift, Thermoacoustics: A Unifying Perspective for Some Engines and Refrigerators, *Springer, Cham* (2017). https://doi.org/10.1007/978-3-319-66933-5
26. N. Rott, Damped and thermally driven acoustic oscillations in wide and narrow tubes, *Z. Angew. Math. Phys.* **20** (1969) 230-243, https://doi.org/10.1007/BF01595562
27. N. Rott, Thermally driven acoustic oscillations. Part II: Stability limit for helium, *Z. Angew. Math. Phys*. **24** (1973) 54-72, https://doi.org/10.1007/BF01593998
28. N. Rott, Thermally driven acoustic oscillations, Part III: Second-order heat flux, *Z. Angew. Math. Phys.* **26** (1975) 43-49, https://doi.org/10.1007/BF01596277
29. N. Rott, Thermoacoustic heating at the closed end of an oscillating gas column, *J. Fluid Mech.* **145** (1984) 1-9, https://doi.org/10.1017/S0022112084002792
30. Z. Zhang, K. Li, J. Ji, Q. Chen and B. Huang, Transient characteristics and thermal boundary effects in standing-wave thermoacoustic refrigerators, *Int. J. Heat Mass Transf.* **236** (2025) 126250, https://doi.org/10.1016/j.ijheatmasstransfer.2024.126250

31. A.I. Abd El-Rahman and E. Abdel-Rahman, Computational fluid dynamics simulation of a thermoacoustic refrigerator, *J. Thermophys. Heat Transf.* **28** (2014) 78-86, https://doi.org/10.2514/1.T4150

32. B.G. Prashantha, M.S. Govinde Gowda, S. Seetharamu and G.S.V.L. Narasimham, Design and comparative analysis of thermoacoustic refrigerators, *Int. J. Air-Cond. Refrig.* **25** (2017) 1750002, https://doi.org/10.1142/S201013251750002X

33. M. E. H. Tijani, Loudspeaker-driven thermo-acoustic refrigeration, Ph.D. Thesis, *Technische Universiteit Eindhoven* (2001), https://doi.org/10.6100/IR547542